NOAA Technical Memorandum GLERL-165

SIMULATION OF ATMOSPHERIC AND LAKE CONDITIONS IN THE LAURENTIAN GREAT LAKES REGION USING THE COUPLED HYDROSPHERE-ATMOSPHERE RESEARCH MODEL (CHARM)

Brent M. Lofgren

NOAA, Great Lakes Environmental Research Laboratory, Ann Arbor, MI

October 2014

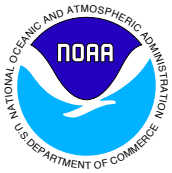

UNITED STATES
DEPARTMENT OF COMMERCE

Penny Pritzker
Secretary

NATIONAL OCEANIC AND
ATMOSPHERIC ADMINISTRATION

Kathy Sullivan
Acting, Under Secretary for Oceans & Atmosphere
NOAA Administrator

NOTICE

Mention of a commercial company or product does not constitute an endorsement by the NOAA. Use of information from this publication concerning proprietary products or the tests of such products for publicity or advertising purposes is not authorized. This is GLERL Contribution No. 1736.

This publication is available as a PDF file and can be downloaded from GLERL's web site: www.glerl.noaa.gov. Hard copies can be requested from GLERL Information Services, 4840 S. State Rd., Ann Arbor, MI 48108.
pubs.glerl@noaa.gov.

NOAA's Mission – To understand and predict changes in Earth's environment and conserve and manage coastal and marine resources to meet our nation's economic, social, and environmental needs

NOAA's Mission Goals:

- Protect, restore and manage the use of coastal and ocean resources through an ecosystem approach to management
- Understand climate variability and change to enhance society's ability to plan and respond
- Serve society's needs for weather and water information
- Support the Nation's commerce with information for safe, efficient, and environmentally sound transportation
- Provide critical support for NOAA's Mission

TABLE OF CONTENTS

LIST OF FIGURES

Simulation of atmospheric and lake conditions in the Laurentian Great Lakes region using the Coupled Hydrosphere-Atmosphere Research Model (CHARM)

Brent M. Lofgren

ABSTRACT. Greenhouse gas-induced climate change will have notable effects on the Great Lakes region, in the atmosphere, land surfaces, and lakes themselves. Simulations of these effects were carried out using the Coupled Hydrosphere-Atmosphere Research Model (CHARM), driven by output from the Canadian General Circulation Model version 3 (CRCM3) for past and future time periods. This results in increased downward longwave radiation and near-surface air temperature. The air temperature increases during summer have strong spatial minima directly over the lakes that are limited to the lowest model layer and seem to be associated with frequent fog depicted by CHARM. Precipitation is also generally increased, with the most spatially coherent, and among the strongest, increases occurring in the near-shore lake effect zones during winter. Evapotranspiration is generally increased, although only weakly over land, but very strongly over the lakes during winter. Water temperatures are increased and the summer stratification pattern (warmer water overlying colder) is established earlier in the year. Ice cover is diminished and limited to shallow parts of the lakes. Several bugs and shortcomings in CHARM are identified for correction in future development and use.

1. INTRODUCTION

Climate change has been noted during the 20th and early 21st centuries through observations.Via mechanisms regarding the behavior of greenhouse gases (GHGs), this change is attributed to human contributions to atmospheric GHG concentrations, with these changes expected to persist and accumulate into the future (IPCC 2013). These changes in climate have a strong potential for affecting aspects of the water resources, ecosystems, and human systems of the Great Lakes basin.

The Laurentian Great Lakes are located on the border between the United States and Canada. They contain about 20% of the world's surface freshwater. Their drainage basin includes 576,000 km^2 of land in addition to the 224,000 km^2 of lake, so that the Great Lakes make up 28% of the total area of their drainage basin, a larger proportion than any large drainage basin.

The water budget of the Great Lakes basin has been a key topic in the investigation of climate change impacts in the region. One of the avenues through which this question has been approached used existing hydrological models in combination with a "change factor" approach to ingesting general circulation model (GCM)-generated meteorological data into these models. This method was originated by Croley (1990) and Hartmann (1990), was extended through a series of papers, and culminated in research by Angel and Kunkel (2010) and Hayhoe et al. (2010). These studies and others using the same methodology generally projected drops in lake levels over multi-decadal to century timescales, although the magnitude varied, and for a minority of particular input datasets of GCM-generated climatic variables, the lake levels did increase. Angel and Kunkel (2010) was particularly comprehensive in the variety of input datasets that it compared, and it produced a range of lake level projections, which were interpreted as a range of uncertainty. However, Lofgren et al. (2011) pointed out significant flaws in this method, centering around the fact that although it is calibrated to adhere to limits resembling the law of conservation of energy at the land surface during the historical calibration period, conservation of energy does not carry over into altered climatic regimes. This flaw leads to excessive evapotranspiration of water from the land surface in future scenarios, which results in over-projection of water level drops on Lake Michigan-Huron by the end of the 21st century by around 1 m. Other methods for projecting the water budget of the Great Lakes basin were used by Manabe et al. (2004) and Milly et al. (2005), both of whom derived net water budgets from the hydrologic schemes inherent within GCMs, and Kutzbach et al. (2005), who calculated atmospheric moisture flux

convergence directly from GCM output. All three of these showed increases in either net basin supply or river outflow, both of which necessarily imply higher lake levels.

The advance of ever-increasing calculation speeds of computer processors and the advance in parallelization, both in terms of hardware and software capabilities, have made regional climate modeling, often referred to as dynamical climate downscaling, more practical. In this approach, state variables including air temperature, pressure, wind, and humidity generated by a GCM are used as lateral boundary conditions (drivers) at the edges of the domain of a regional climate model (RCM). An ambitious project for taking this approach to climate simulation across a domain encompassing nearly all of North America, and using many combinations of GCM input and RCM, is the North American Regional Climate Change Assessment Program (NARCCAP, Mearns et al. 2009). In general, the NARCCAP simulations did not explicitly include two-way interaction between the temperature, thermodynamics, and (even simplified) dynamics of the Great Lakes, on one hand, and the radiation, thermodynamics, and dynamics of the atmosphere.

Several studies have taken the regional climate modeling approach on domains that specifically focus on the Great Lakes basin. Lofgren (2004) was an early attempt at validating an RCM, coupled to a simple process model of lake thermodynamics, for Great Lakes application. MacKay and Seglenieks (2013) simulated the Great Lakes basin using the Canadian Regional Climate Model (CRCM) and incorporating a single-layer "slab" model of the Great Lakes' thermodynamics, and proceeded to estimate the overall water budget implications of climate change. Bennington et al. (2014) and Notaro et al. (2014) used the Regional Climate Model version 4 (RegCM4) in conjunction with the 1-dimensional lake heat diffusion scheme of Hostetler and Bartlein (1990) to simulate Great Lakes regional climate and estimate resultant water budgets. Gula and Peltier (2012) used a version of the Weather Research and Forecasting (WRF) model to downscale Great Lakes regional climate; their treatment of the lake surfaces themselves was to adjust their surface temperatures in accordance with the air temperature anomalies (relative to historical time periods) within the driving GCM. Music et al. (2014) gives a summary of the validation in the Great Lakes region of several individual model runs related to NARCCAP.

2. MODEL FORMULATION

The description of the formulation of CHARM here is a revision of that in Lofgren (2004). Primary changes include the use of an updated version of the Regional Atmospheric Modeling System (RAMS) and the substitution of the formulation of Hostetler and Bartlein (1990) for vertical diffusion of heat within the lakes' water column on a spatially distributed basis in place of a parameterization of the lake thermodynamics that treats each lake as a single, spatially lumped column. The atmospheric dynamical core of CHARM is comprised of RAMS version 6.0 (Pielke et al. 1992, Cotton et al. 2003). This system models the atmosphere using the primitive equations of motion implemented on an Arakawa C grid placed on a stereographic map projection. We used a grid with 40 km grid spacing in the projected plane centered at 45° N, 84° W, with 72 grid points in the x-direction (approximately east-west) and 64 in the y-direction (true north-south along the center line, approximate elsewhere). This domain covers the entire Great Lakes basin, plus a generous buffer zone in all directions to increase the distance between the area of interest and the effects of non-physical phenomena that tend to appear near the boundaries of limited-area atmospheric models.

In the vertical coordinate, there are 24 sigma-z levels. Sigma-z levels transition from approximating distance above ground level near the surface to approximating distance above mean sea level near the vertical limit of the domain. The lowest level is specified as being 100 m thick, with each successive level being 1.2 times as thick as the next lower, to a maximum of 1900 m thick. This places the top of the model at 23,893 m above mean sea level—well above the tropopause.

The model state variables of potential temperature, water vapor mixing ratio, pressure, and horizontal wind components are nudged toward input values near the outer edges and in the upper part of the model (see section 3 for a description of the input dataset). The outermost grid points on each edge have their values nudged toward the input values with a relaxation time of 15 minutes; the strength of nudging is reduced linearly toward zero at a distance of 400 km (10 grid

spaces) from the outer edge. Additionally, values are nudged in the upper part of the domain, with a relaxation time of 30 minutes at the top of the model domain, with nudging strength reducing linearly to zero at 5,000 m sigma-z height. The land surface hydrology module in RAMS uses a formulation of a column of soil as described in Tremback and Kessler (1985). The vegetation is treated using a "big leaf" scheme based on Avissar and Pielke (1989) and described in more detail in Tremback (2005). Soil moisture was initialized to a value of 0.6 times the local value of saturated soil moisture. Resultant time series of soil moisture show that it relaxes to a dynamic equilibrium state within one year of initializing the model.

We have added to the RAMS formulation a provision for water to percolate through the bottom of the actively evaporating soil column in a manner consistent with the formulation of the rest of the soil column. Furthermore, we keep an account of the quantity of this percolation as well as the amount of surface runoff that occurs (surface runoff was already calculated within RAMS, but an account of its quantity was not saved). As a post-processing step, we have used a sharply truncated version of the Large Basin Runoff Model (LBRM) of Croley (1983). Because CHARM includes calculation of evapotranspiration from the land surface, we use only two of the storage reservoirs of the LBRM: the groundwater storage and the surface storage. The input to the groundwater storage is the percolation from the bottom of the active soil layer as calculated by CHARM and averaged over each of the Great Lakes drainage sub-basins according to the area of each CHARM grid cell that overlaps with each sub-basin. The input to the surface storage reservoir is the outflow from the groundwater storage plus the surface runoff determined by CHARM, again averaged over the area of each sub-basin. The outflow from the groundwater storage and surface storage are each derived by treating each as a linear reservoir, multiplying each by an empirical coefficient determined by calibration of the full LBRM model. The resultant time series of outflow from the surface storage will be regarded as each sub-basin's contribution to the net basin supply for the corresponding lake. However, analysis from this post-processing module is not shown in this report because of suspected errors in its coding and overall deficiency in model precipitation.

A lake component is also incorporated into CHARM. It is based on the model of Hostetler and Bartlein (1990). In this model component, the water column in each of the CHARM grid cells that are within the Great Lakes is treated independently. The heat fluxes at the surface--shortwave and longwave radiation, sensible heat flux, and latent heat flux, are calculated and used to adjust the temperature of the layer of water closest to the surface. This is accompanied by vertical mixing of the water column, whose strength is a function of wind speed above the water and vertical stability of the water column. The main departure of our formulation from that of Hostetler and Bartlein (1990) is in the calculation of the coefficient of decay of the Ekman spiral. In their equation (7),

$$k^* = 6.6\left(\sin\phi\right)^{\frac{1}{2}} U_2^{-1.84} \quad . \tag{1}$$

Here, k* is the coefficient of decay of the Ekman spiral with depth, in units of inverse meters, ϕ is latitude, and U_2 is wind speed (m/s) measured at 2 m above the surface. In running CHARM, the wind speed that is used is from the mid-level of lowest atmospheric layer, approximately 47.7 m above the ground. To adjust for this difference in measurement height, and for use as a tuning parameter, the 47.7 m value of wind speed is multiplied by a coefficient before insertion into eq. (1). The coefficient that gave an approximate match between the seasonal cycle of simulated and observed lake-mean surface temperatures was 0.28 (see validation of lake surface temperatures in section 5.1).

3. EXPERIMENTAL DESIGN

The experimental model runs involve two time slices of simulation, representing the historical years 1964-2000 and future projections for 2043-2070. Because the underlying RAMS model has coding that allows its time counter to count up to 2^{29} seconds, or just over 17 years, each time period was subdivided into multiple individual model runs. The driving GCM retains memory via certain global-scale aspects of the system, notably ocean temperatures and dynamics, but CHARM needs some time to spin up the lake thermodynamics and soil moisture portions of the model. Thus we ran the periods 1962-1978, 1977-1993, and 1992-2000, and discarded the first two years' output from each segment. Likewise, we ran

2041-2057 and 2056-2070 and discarded the first two years' output from these. The two overall time periods will be referred to as the 1982 time slice and the 2055 time slice, for the years on which they are centered.

The input data used for nudging of model variables near the lateral edges of the domain and at higher altitudes were taken from a run of the Canadian Regional Climate Model (CRCM, Music and Caya 2007, de Elia and Côté 2010), completed at Ouranos (research institution in Montréal). This model was run with a domain covering all of North America and the surrounding oceans at 45 km grid spacing. The model was forced in turn by a run of the Coupled General Circulation Model version 3 (CGCM3, Flato and Boer 2001) of the Canadian Centre for Climate Modelling and Analysis. These were run under observed CO_2 concentrations during the historical period and under the A2 emission scenario (IPCC 2000) in the future.

Time-variable concentrations of CO_2 were also used within CHARM. To approximate the observed values, for the historical times we used the formula 310 + 1.5 (y - 1960) to give the CO_2 concentration in parts per million by volume during year y. For the future, we used 471 + 5.9 (y - 2040) to approximate the A2 scenario.

4. ATMOSPHERIC RESULTS

4.1 Air temperature - validation with observations

Air temperatures simulated by CHARM at 2 m height during the 1964-2000 time period are compared (Figs. 1 and 2) with spatially interpolated air temperatures from the station-based air temperature data in GLERL's hydro-climate database, which in turn is derived from Summary of Day data from the cooperative observer network, as distributed by the National Climatic Data Center. Interpolation used inverse distance weighting incorporating all stations within 80 km of the center of the corresponding grid cell of CHARM, while grid cells with no reporting stations within 80 km were flagged as having no data. Because of the low spatial coverage over much of Canada, and selection of stations for those in or near the Great Lakes basin, some areas, indicated by dark blue, have no data (i.e. no stations reporting within 80 km of the center of the corresponding CHARM grid cell). During June, July, and August (JJA), air temperatures at 2 m above the surface differ between observations and simulations by less than 2°C over nearly all land areas, and many areas show even closer agreement (Fig. 1). CHARM simulates colder temperatures directly over the lakes relative to nearby land areas. This is physically reasonable, but because the observational dataset does not include over-lake locations, validation of the magnitude of this lake signature in temperature is uncertain.

During December, January, and February (DJF), near-surface air temperatures again show good agreement between observations and CHARM over most land areas (Fig. 2). Over the lower peninsula of Michigan, the temperatures in CHARM are biased about 2°C warmer than in the observations, and somewhat larger biases occur in northern New York State, but in most land areas the biases are well below 2°C. CHARM's air temperatures over the Great Lakes are warmer during winter than nearby land areas, by about 4-6°C, but again, lack of over-lake observations does not allow for validation of this magnitude). And there are small areas of warmer air temperatures over some of the larger lakes other than the Great Lakes, such as Lake Nipigon north of Lake Superior, and Lake of the Woods near the northwestern corner of the figure's domain.

4.2 Air temperature change

Near-surface air temperature during JJA is increased in the 2043-2070 period relative to 1964-2000 due to increased GHG concentration, by amounts ranging from 2.4 to 4.1°C (Fig. 3). There is a general gradient in which areas further south have larger temperature increases than those further north. Additionally, there is a strong signature of smaller temperature increases over the Great Lakes. This lake signature is almost entirely confined to the lowest model layer (not shown). The presence of frequent fog (occurring for some portion of nearly every day) in the lowest model layer during the summer, primarily during the day, seems to be a major contributor to this minimum in temperature increase, via the following mechanism, schematically illustrated in Fig. 4.

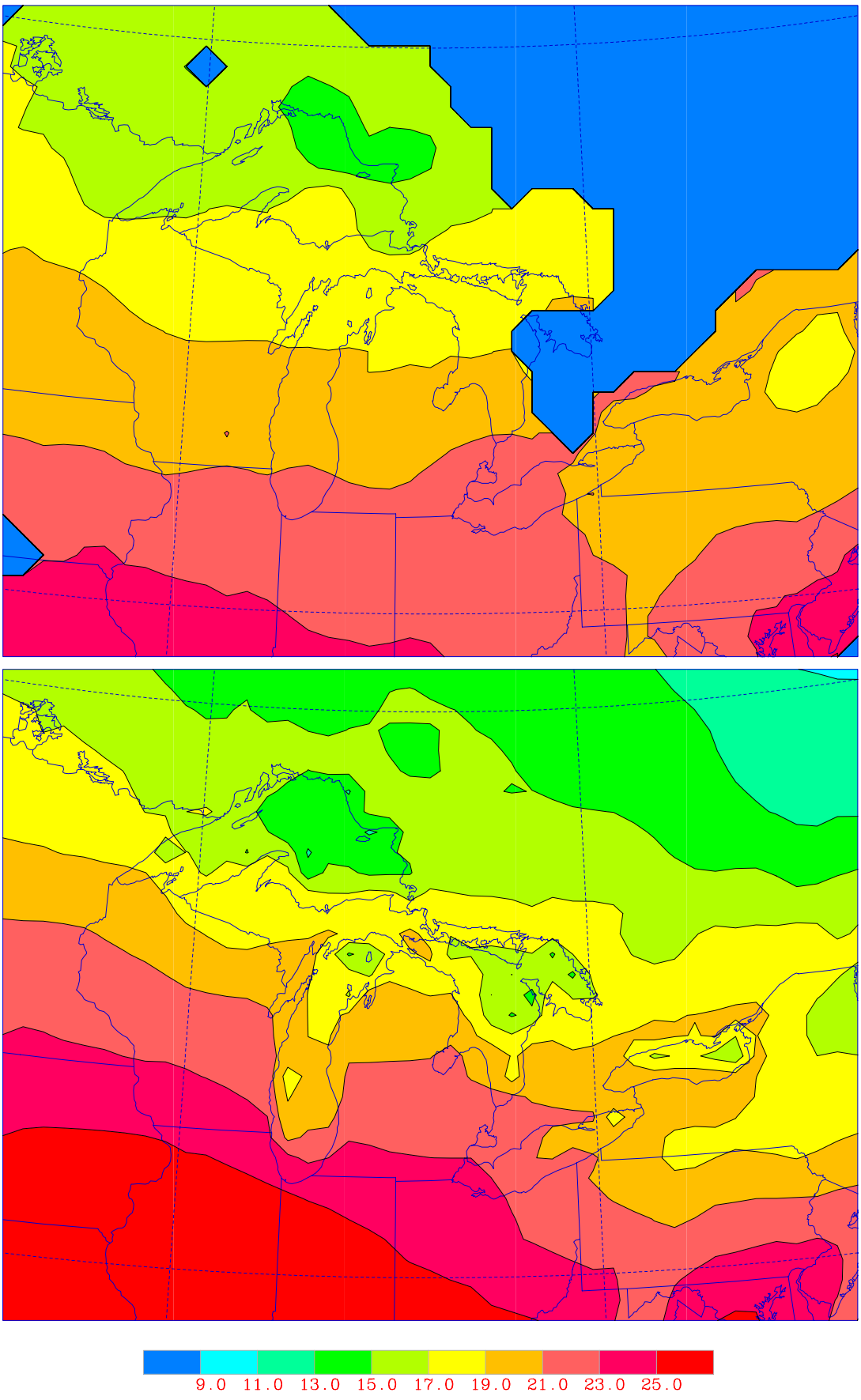

Figure 1. (Top) Spatially interpolated near-surface air temperatures (degrees C) during June, July, and August (JJA) of 1964-2000 based on station observations in GLERL's hydro-climate database. Dark blue indicates no data within 80 km. (Bottom) Near-surface air temperature during JJA as simulated by CHARM during the historical period.

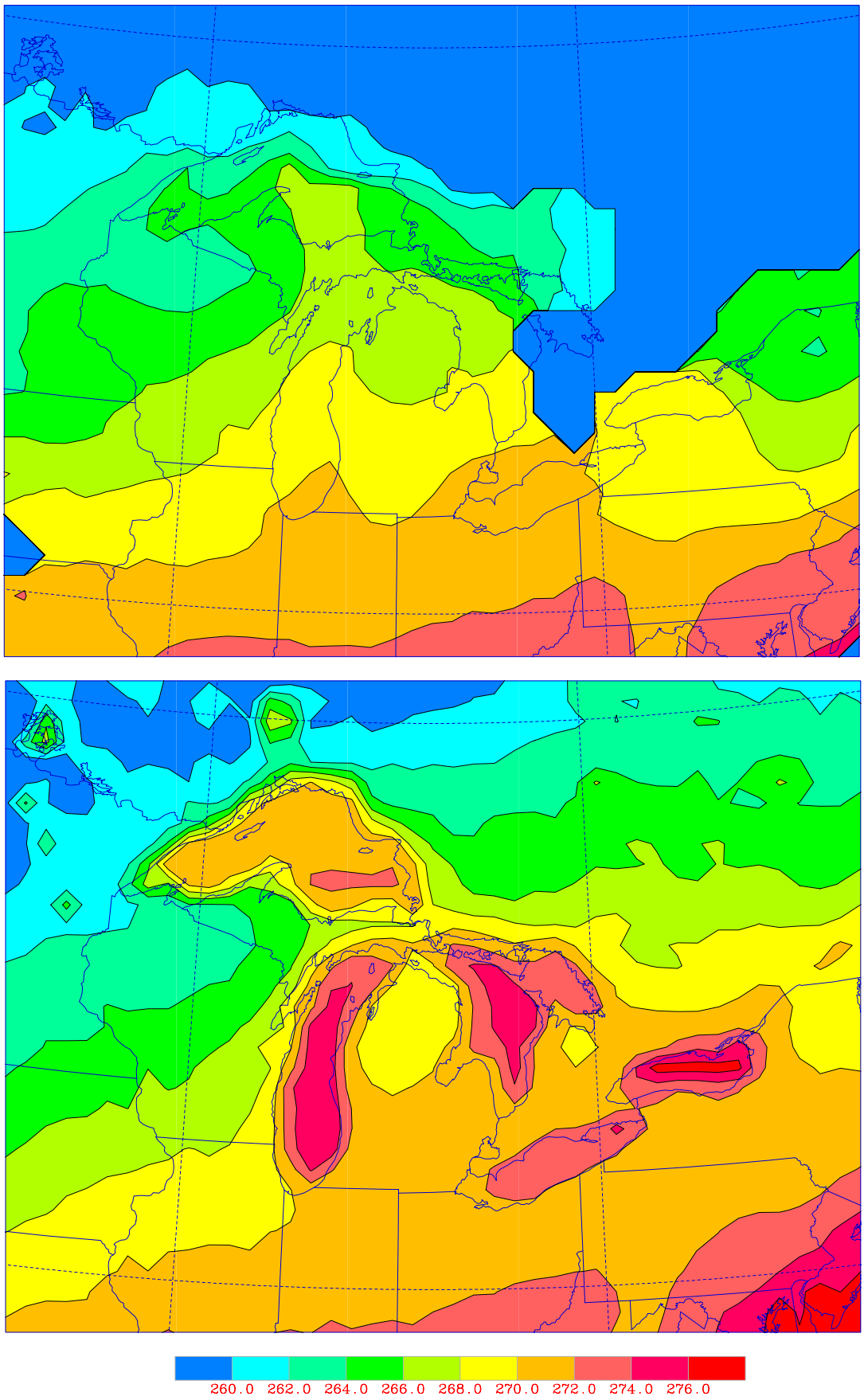

Figure 2. (Top) Spatially interpolated near-surface air temperatures (degrees C) during December, January, and February (DJF) of 1964-2000 based on station observations in GLERL's hydro-climate database. Dark blue indicates no data within 80 km. (Bottom) Near-surface air temperature during DJF as simulated by CHARM during the historical period.

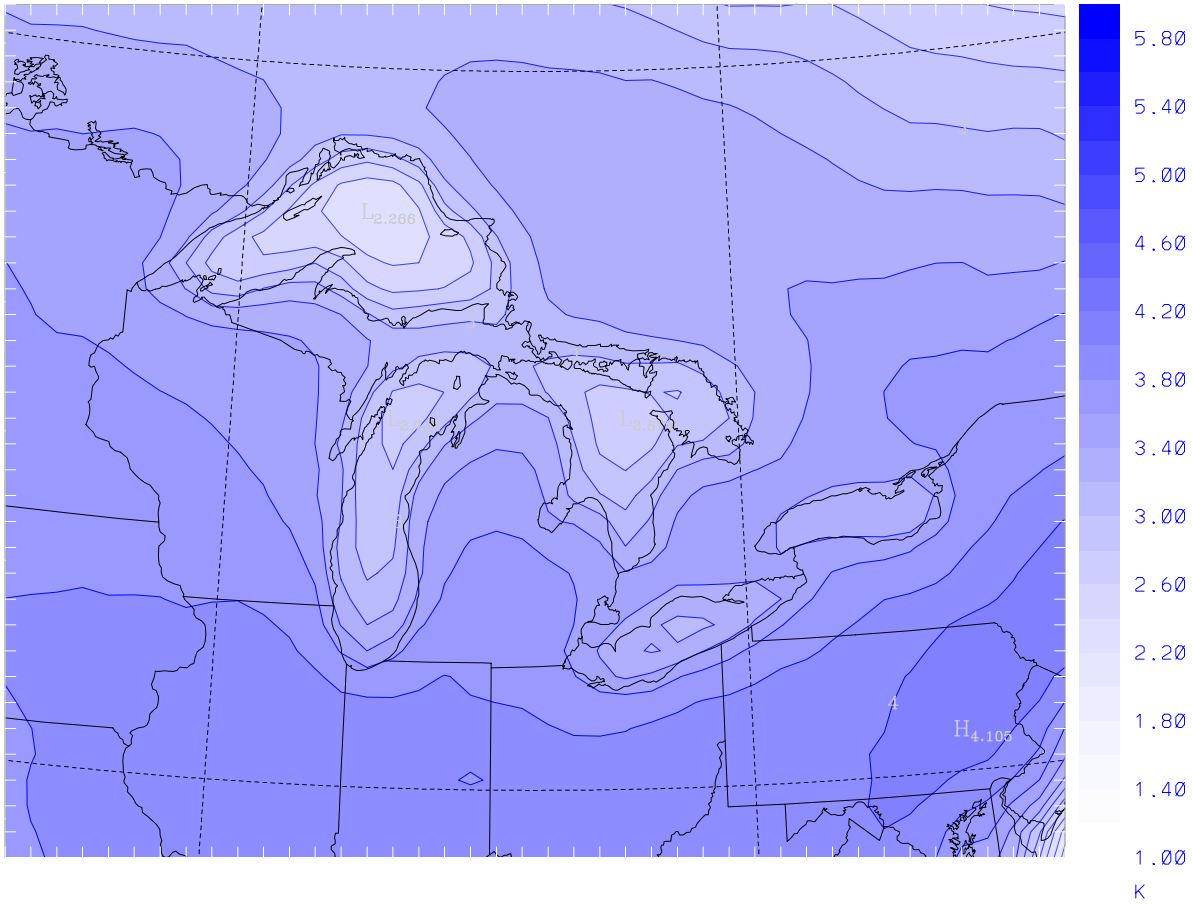

Figure 3. Change in CHARM-simulated near-surface air temperatures (degrees C) during June, July, and August for the 2043-2070 period minus 1964-2000.

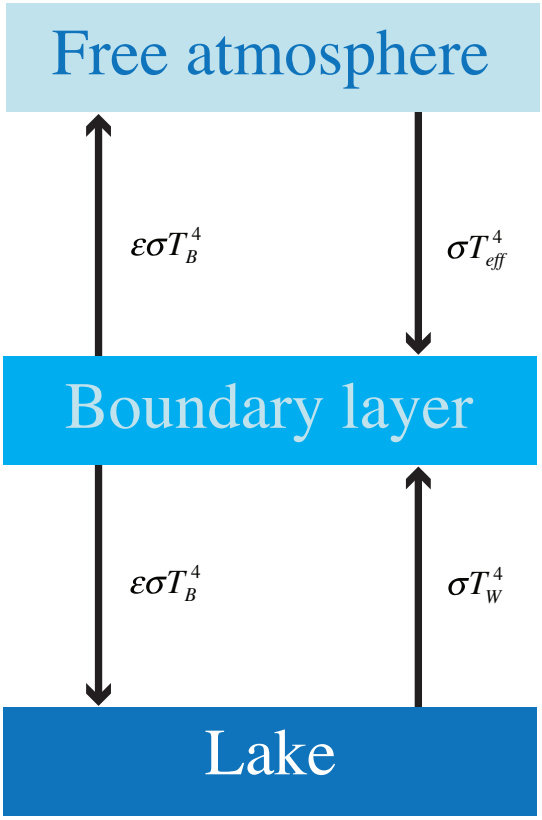

Figure 4. Schematic depiction of longwave radiative heat fluxes that may cause cooling of the atmospheric boundary layer due to increased fog.

If we assume that the emissivity of the water surface is close to unity, and combine the effects of emissivity and temperature of all the layers of air above the boundary layer to get an effective temperature such that the downward longwave radiation at the top of the boundary layer is σT_{eff}^4, the contribution of longwave radiation to the temperature tendency in the boundary layer is:

$$\varepsilon\sigma\left(T_W^4 + T_{eff}^4 - 2T_B^4\right) / \, pc_p\Delta z \tag{2}$$

where ε is the emissivity of the boundary layer, T_W is the temperature of the water surface, T_{eff} is the effective temperature of the free atmosphere, T_B is the temperature of the boundary layer, ρ is the air density, c_p is the heat capacity of air, and Δz is the thickness of the boundary layer. T_W and T_B are close in value, but T_{eff} is smaller, typically by a large margin. Therefore, the quantity inside the parentheses is always negative, and increasing the value of ε, or the duration during the day in which high emissivity of the boundary layer occurs, exerts a cooling effect on the boundary layer. The lowest model layer in stable summertime conditions is reasonably well coupled to the water surface, but dynamically interacts only weakly with higher levels, and thus can be considered the entire boundary layer, so the small value of Δz contributes to the strength of this effect on near-surface temperatures, and lack of effect at higher levels. This mechanism seems to be associated with CHARM's tendency to produce overlake fog of excessive extent and duration during the summer, despite the modification of the water surface surface flux formulation to eliminate all evaporation when condensed water is present in the lowest atmospheric layer. The resulting change in the temperature of both the lake surface and over-lake near-surface air also seem to be at odds with the observations of Austin and Colman (2007), who showed that surface temperatures of Lake Superior during the summer have increased much more quickly than surface air temperatures at nearby land stations.

The temperature differences between the 2043-2070 and 1964-2000 time periods for DJF have smaller overall magnitudes, ranging from 1.5 to 3.2°C (Fig. 5). In this season, the overall meridional gradient is reversed, with larger temperature increases occurring in regions farther north.

4.3 Precipitation—validation with observations

CHARM's precipitation during JJA is strongly dry biased during the historical period (Fig. 6). The figure shows precipitation on a logarithmic scale (each consecutive contour differs by a factor of 2). Therefore, most areas have CHARM precipitation reduced by a factor between 2 and 4 relative to observations. A combination of factors is likely contributing to this: 1) low incoming moisture flux in the lateral boundary conditions provided by the CGCM3 dataset, 2) a need for further tuning of the convective precipitation scheme (the dominant mechanism for summer rainfall), and 3) a positive feedback mechanism in which low precipitation leads to low soil moisture, in turn leading to low evapotranspiration and atmospheric humidity, and further reduced precipitation.

During DJF, precipitation is still biased dry, but not as severely (Fig. 7). Some southern and eastern portions of the domain have precipitation underestimated by nearly a factor of 2, but much of the western and northwestern part of the domain is nearly bias-free. The mechanism of low incoming moisture flux due to the boundary conditions may well be active during winter. But convective precipitation and regional land-based evapotranspiration are small contributors to wintertime precipitation, so these factors are much less important than during summer. Because lake-effect precipitation occurs locally at near-shore land stations, some of this signature appears in the winter observations, although the logarithmic scaling may be obscuring some of the features. Lake-effect precipitation is evident in the observations over the Keweenaw Peninsula on the southern shore of Lake Superior, at the eastern shore of Lake Superior, at the eastern shore of Georgian Bay (partially obscured by the region of no data), a bulge in the contour just east of southern Lake Michigan, and just east of Lake Ontario. In the CHARM results, the main lake-effect signature that is evident is the closed contour surrounding the eastern shore of Lake Michigan.

4.4 Precipitation change

During JJA, precipitation is generally increased, but the spatial distribution of its magnitude is patchy, reflective of the inhomogeneous nature of the convective cell-dominated summer precipitation (Fig. 8). Some of the larger magnitudes of

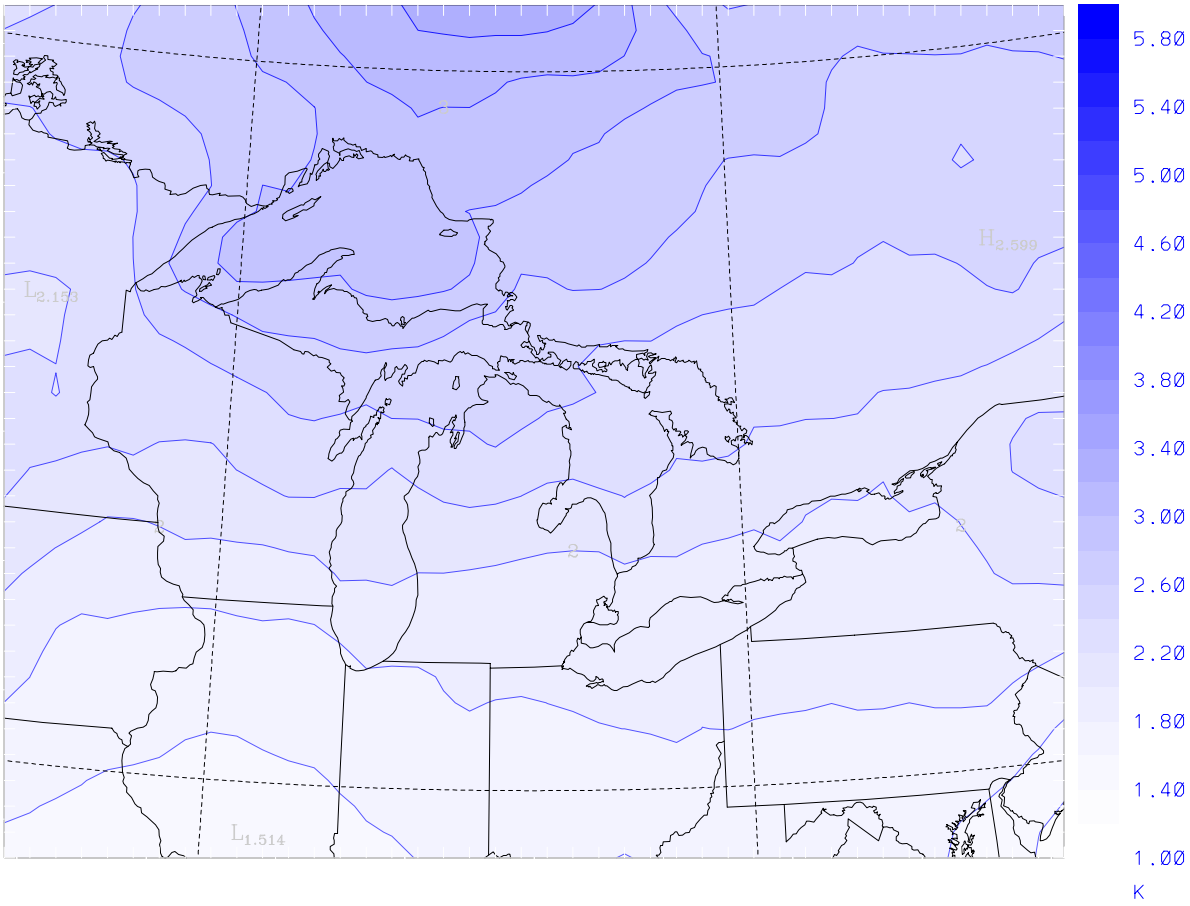

Figure 5. Change in CHARM-simulated near-surface air temperatures (degrees C) during December, January, and February for the 2043-2070 period minus 1964-2000.

increase appear to occur downwind (relative to prevailing westerlies) of Lake Michigan in the northern lower peninsula of Michigan, and to the east of Georgian Bay. There is a rather large but isolated patch of decreased precipitation directly over southern Lake Michigan.

During DJF, precipitation is increased throughout the domain, but the regions of highest magnitude of increase have a strong lake-related signature (Fig. 9). Lakes Superior, Huron, and Ontario have their strongest increases in precipitation over the eastern extremes of the lakes, and extending to the adjacent land. Lake Erie has a somewhat attenuated version of this pattern, while Lake Michigan has a much weaker signal. It may be that under prevailing north-westerly wind conditions, long fetches over Lake Superior lead to strong boundary layer instability, and that this can also pre-condition lake-effect precipitation over Lakes Huron and Ontario. However, such pre-conditioning will affect Lake Erie less and Lake Michigan not at all except in the case of wind almost directly from the north.

4.5 Evapotranspiration

During JJA, evapotranspiration (ET) is mostly increased, but the magnitude is not large (Fig. 10). Over land, except for an area north of Lake Huron, the magnitude of this increase is less than 0.2 mm/day. Increases of greater magnitude over the lakes are primarily in the shallow parts of the lake. This is most evident in Lake Superior, where the darker colors are located in stripes near the northern and southern shores, while reduced ET occurs near the center of Lake Superior. ET is also reduced over much of the land in the eastern and southeastern parts of the domain, where precipitation is also reduced, so this can be attributed to moisture limitation.

During DJF, the change in ET over land is of mixed sign and generally between -0.2 and +0.2 mm/day, with a few larger positive values occurring in the southern part of the domain (Fig. 11). Over the lakes, ET is increased by larger

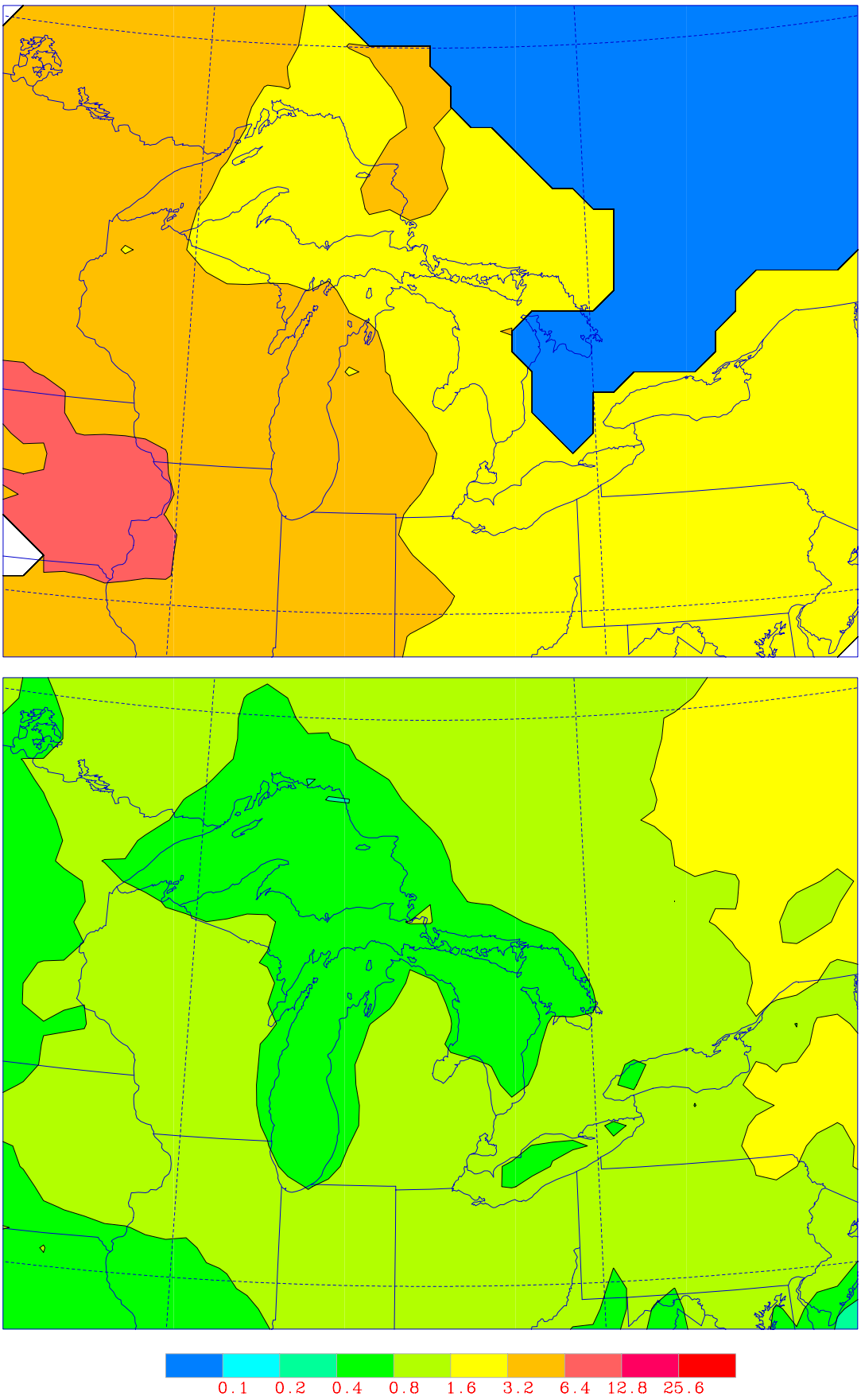

Figure 6. (Top) Spatially interpolated precipitation rate (mm/day) during June, July, and August based on station observations in GLERL's hydro-climate database. Dark blue indicates no data within 80 km. (Bottom) Precipitation rate during JJA as simulated by CHARM during the historical period (1964-2000).

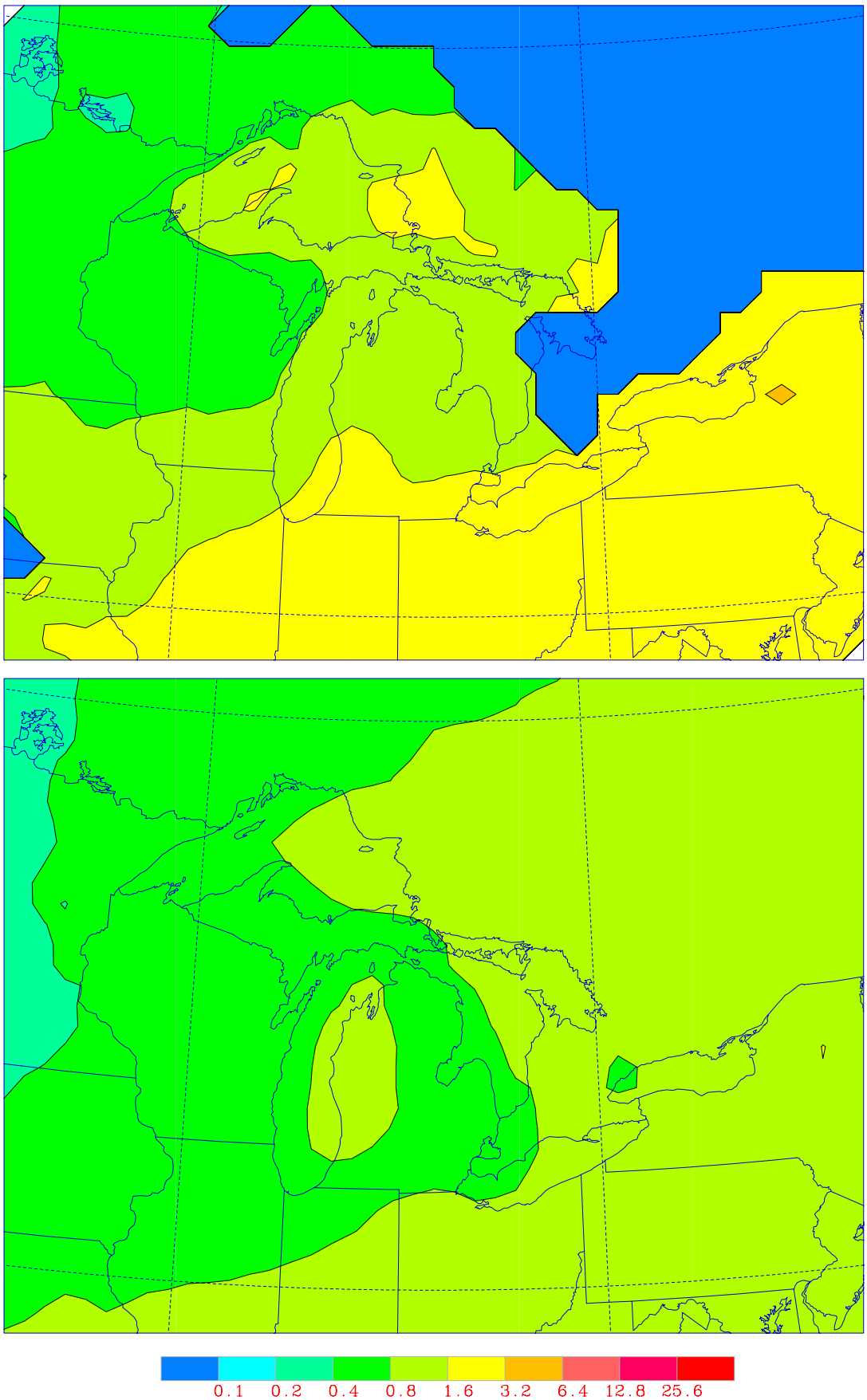

Figure 7. (Top) Spatially interpolated precipitation rate (mm/day) during December, January, and February based on station observations in GLERL's hydro-climate database. Dark blue indicates no data within 80 km. (Bottom) Precipitation rate during DJF as simulated by CHARM during the historical period (1964-2000).

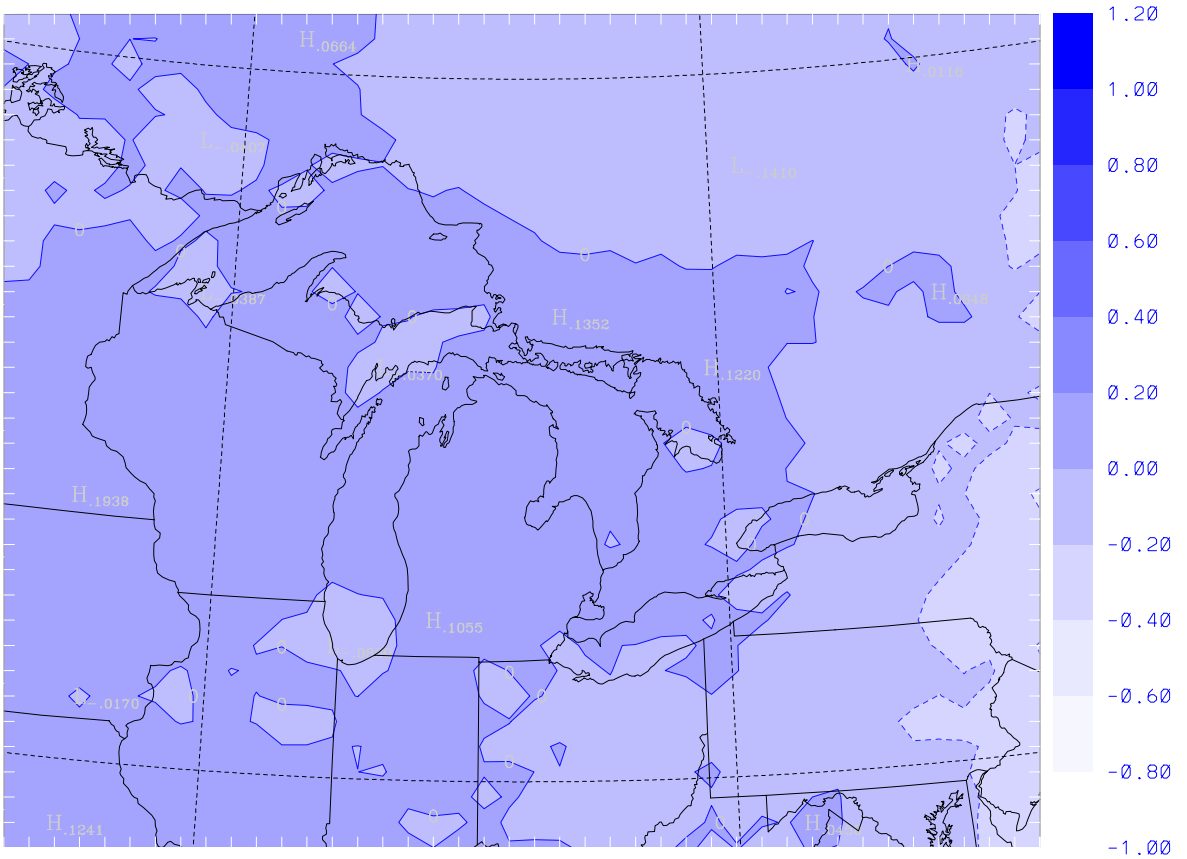

Figure 8. Change in CHARM-simulated precipitation rate (mm/day) during June, July, and August for the 2043-2070 period minus 1964-2000.

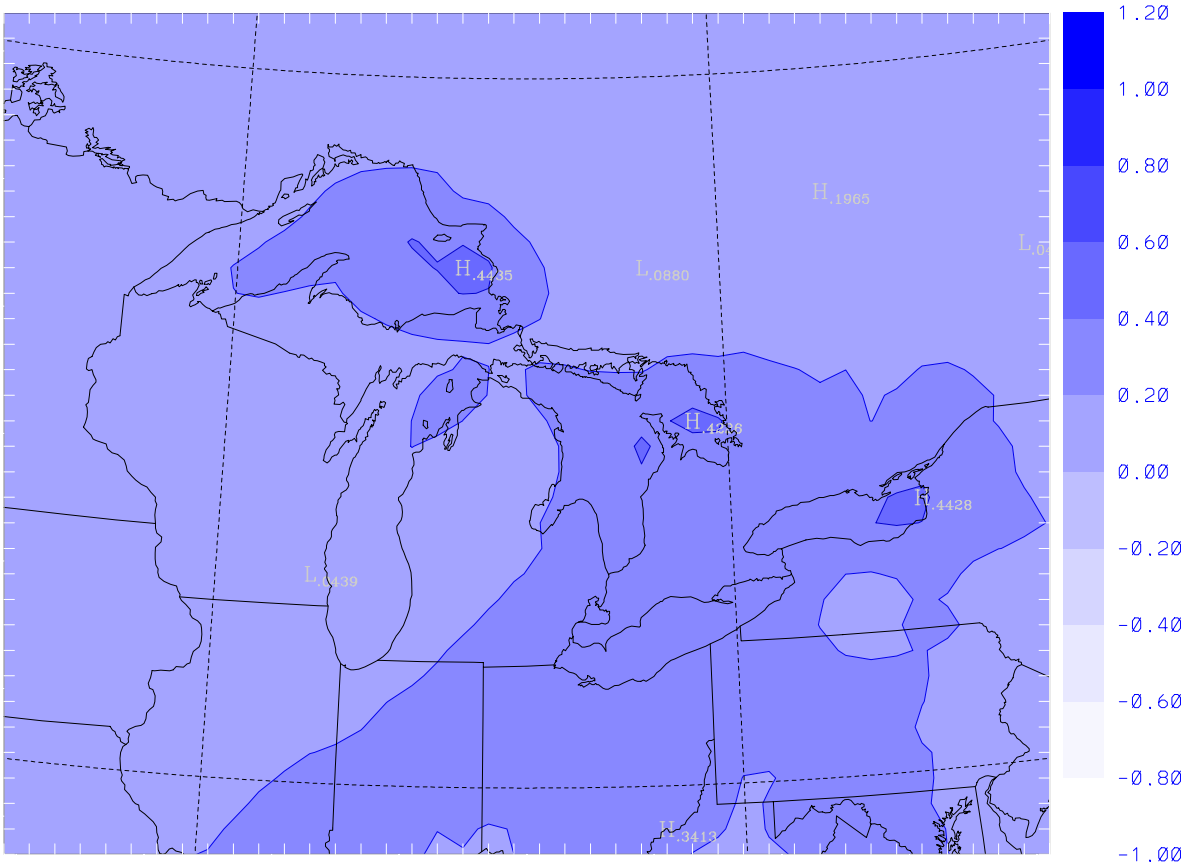

Figure 9. Change in CHARM-simulated precipitation rate (mm/day) during December, January, and February for the 2043-2070 period minus 1964-2000.

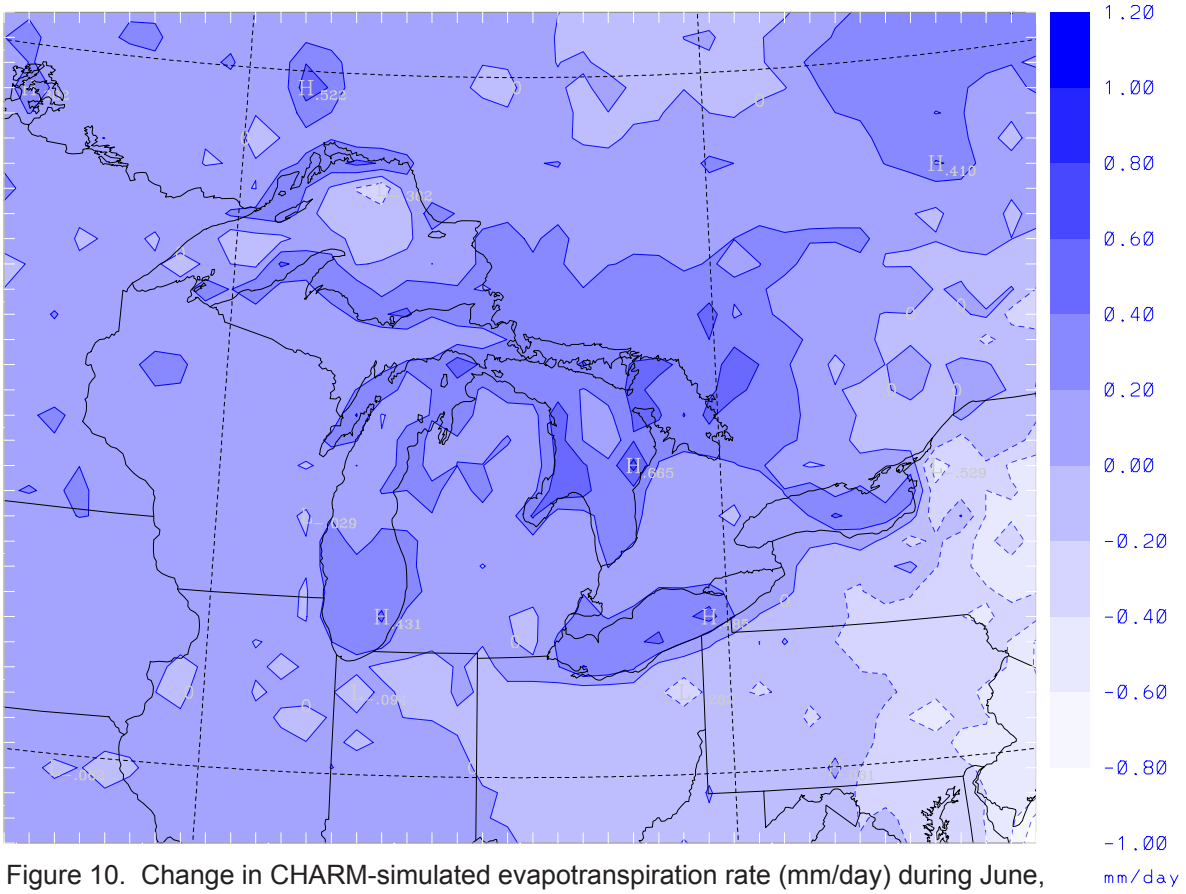

Figure 10. Change in CHARM-simulated evapotranspiration rate (mm/day) during June, July, and August for the 2043-2070 period minus 1964-2000.

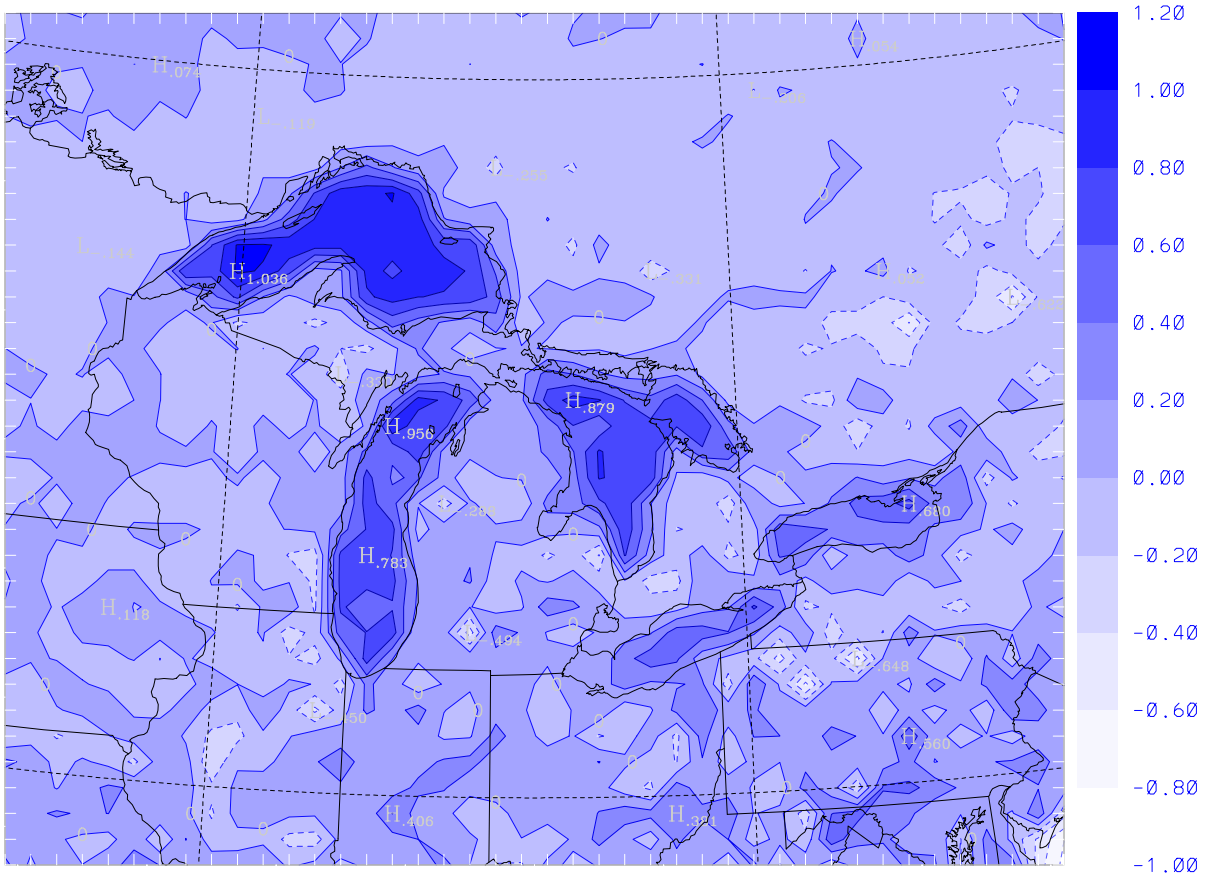

Figure 11. Change in CHARM-simulated evapotranspiration rate (mm/day) during December, January, and February for the 2043-2070 period minus 1964-2000.

magnitudes. The main driving factor behind this is the enhanced storage of heat in the lakes in the future period. Because the boundary layer above the lakes is unstable in this season, this energy is released through turbulent fluxes, much of it in the form of ET accompanied by latent heat flux. This moisture can then be strongly carried into the free atmosphere via turbulence, or be advected toward land, often resulting in lake-effect precipitation and self-reinforcing circulation driven by the latent heat release of this precipitation (see, e.g. Niziol et al. 1995).

4.6 Lake-induced seasonal-mean surface winds

Near-surface winds for the summer during the 1964-2000 time period (not shown) are influenced by the superposition of three main factors: weak geostrophic flow from west to east at the continental/global scale, geostrophic flow in an anti-cyclonic (clockwise) direction encompassing all of the Great Lakes (a diameter of order 1000 km), and flow patterns at smaller scales representing ageostrophic departures from these patterns, generally from lake toward land. These patterns can be thought of as having a Rossby number somewhat below unity at the scale of the entire Great Lakes basin, but greater than unity at the scale of individual lakes and intervening land areas (see Sousounis and Fritsch 1994). Another way of thinking of the lake scale is that a typical air parcel near the surface might traverse Lake Michigan in about 4 hours, compared to the inertial time scale of 17 hours.

The change in simulated near-surface flow during JJA for the future relative to the base period has a variety of features (Fig. 12). Over Lake Michigan, the northward flow of the base period is enhanced, and also has an added westward component. This is driven by a more stable boundary layer in the future than the past and a more intense thermally-driven high pressure center over the lake. Northward anomalies are also pronounced over the northern parts of Lakes Superior and Michigan. These anomalies over Lakes Superior, Michigan, and Huron all represent counter-clockwise rotations of the wind direction, relative to the 1964-2000 period. Thus they do not seem to be due to reduced friction under an Ekman spiral effect, i.e. balance among forces due to pressure gradient, friction, and coriolis effect. Instead, these anomalies are attributable to changes in pressure—mostly thermally direct ageostrophic flow.

During the winter (DJF), similar factors control general near-surface wind pattern (not shown), but with different magnitude and, for the lake-driven factors, different sign as well. The continental-scale background flow is a stronger eastward flow than during summer, there is a cyclonic (counter-clockwise) pattern superimposed at the scale of the full lake basin, and thermally-driven flows at the scale of the lakes go toward the lakes. The simulations for 2043-2070 (Fig. 13) show enhanced southward flow over western Lake Superior and most of Lake Michigan, corresponding to an enhancement of the cyclonic flow at the basin-wide scale, relative to 1964-2000. The southward anomaly over Lake Michigan is also consistent with the flow anomalies over land areas extending to the southwest. Lakes Huron, Erie, and Ontario have westward anomalies, representing a diminution of the background eastward flow at the continental/global scale. An overall decrease in time-mean surface westerlies at mid-latitudes is a generally anticipated result of climate change. This effect is concentrated over the lakes, especially Lake Erie, possibly because of boundary layer and stability effects.

4.7. Downward longwave radiation

Downward longwave radiation sits at the root of the greenhouse effect that drives human-caused climate change. As expected from a case with increased greenhouse gases, downward longwave radiation is increased throughout the domain in the 2043-2070 period. During JJA (Fig. 14), the increases in the domain are mostly in the range of 10-30 W/m^2. The lakes themselves, especially Lake Michigan, have a signature of a slightly smaller increase in downward longwave radiation than the adjacent land. This indicates that the greater emissivity from more low-level clouds is offset by the lesser increase in fog and low-level air temperature over the lakes.

During DJF, downward longwave radiation in the region is generally increased by 10-20 W/m^2, with a small area over Lake Superior exceeding 20 W/m^2. The magnitude of increased downward longwave radiation is greater over the lakes than over adjacent land. This is attributable to a combination of greater increase in air temperature over the lakes, and greater enhancement of the greenhouse effect due to the input of water vapor from the lakes into the lower atmosphere.

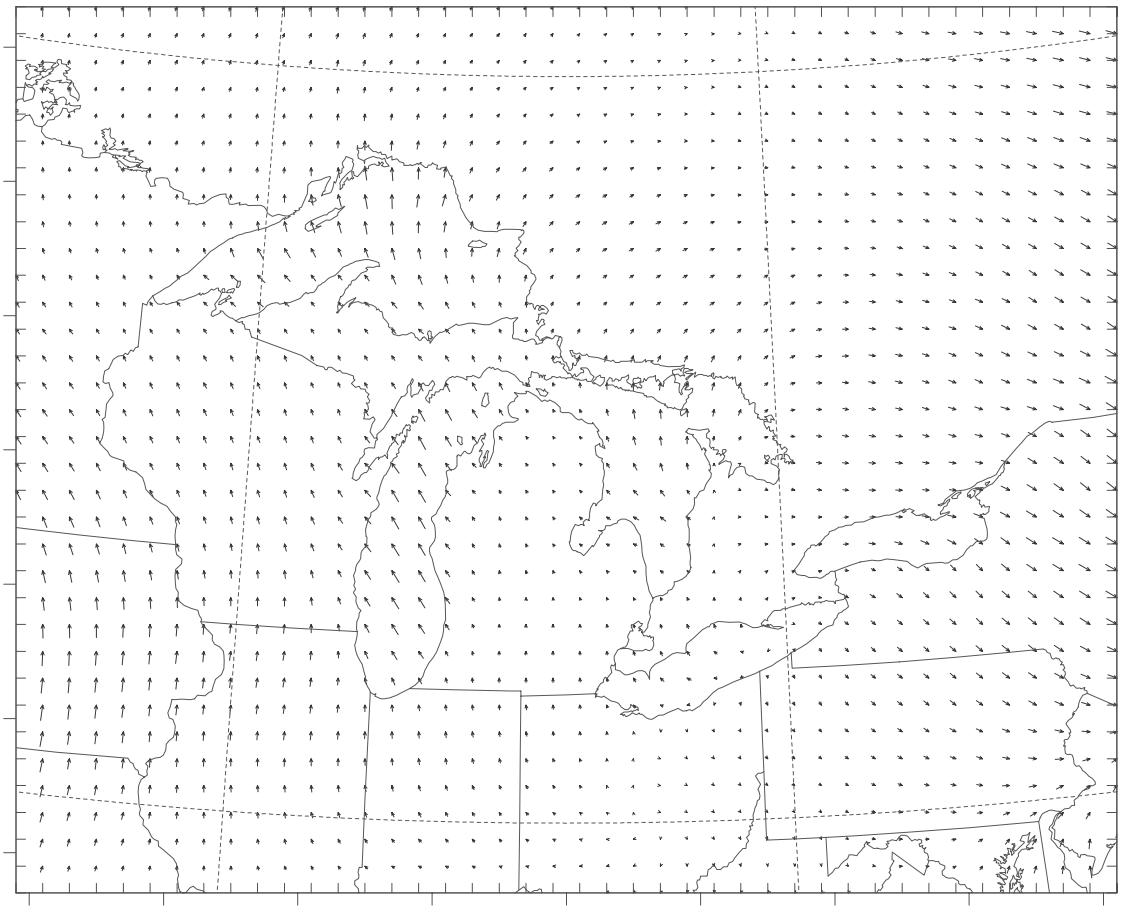

Figure 12. Change in CHARM-simulated mean wind vector during June, July, and August at the lowest model level (48 m above the surface)—2043-2070 minus 1964-2000. An arrow of length equal to the distance between the grid points displayed represents a magnitude of 1 m/s.

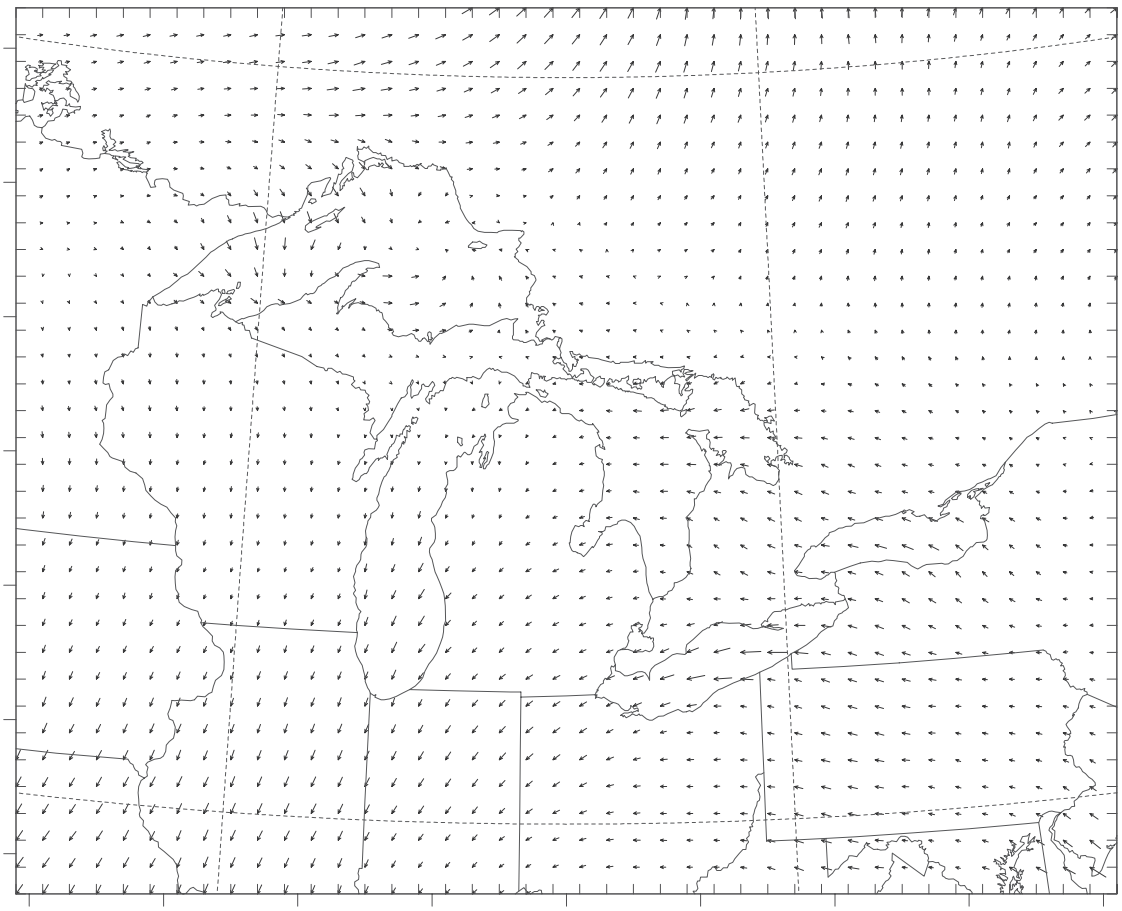

Figure 13. Change in CHARM-simulated mean wind vector during December, January, and February at the lowest model level (48 m above the surface)—2043-2070 minus 1964-2000. An arrow of length equal to the distance between the grid points displayed represents a magnitude of 1 m/s.

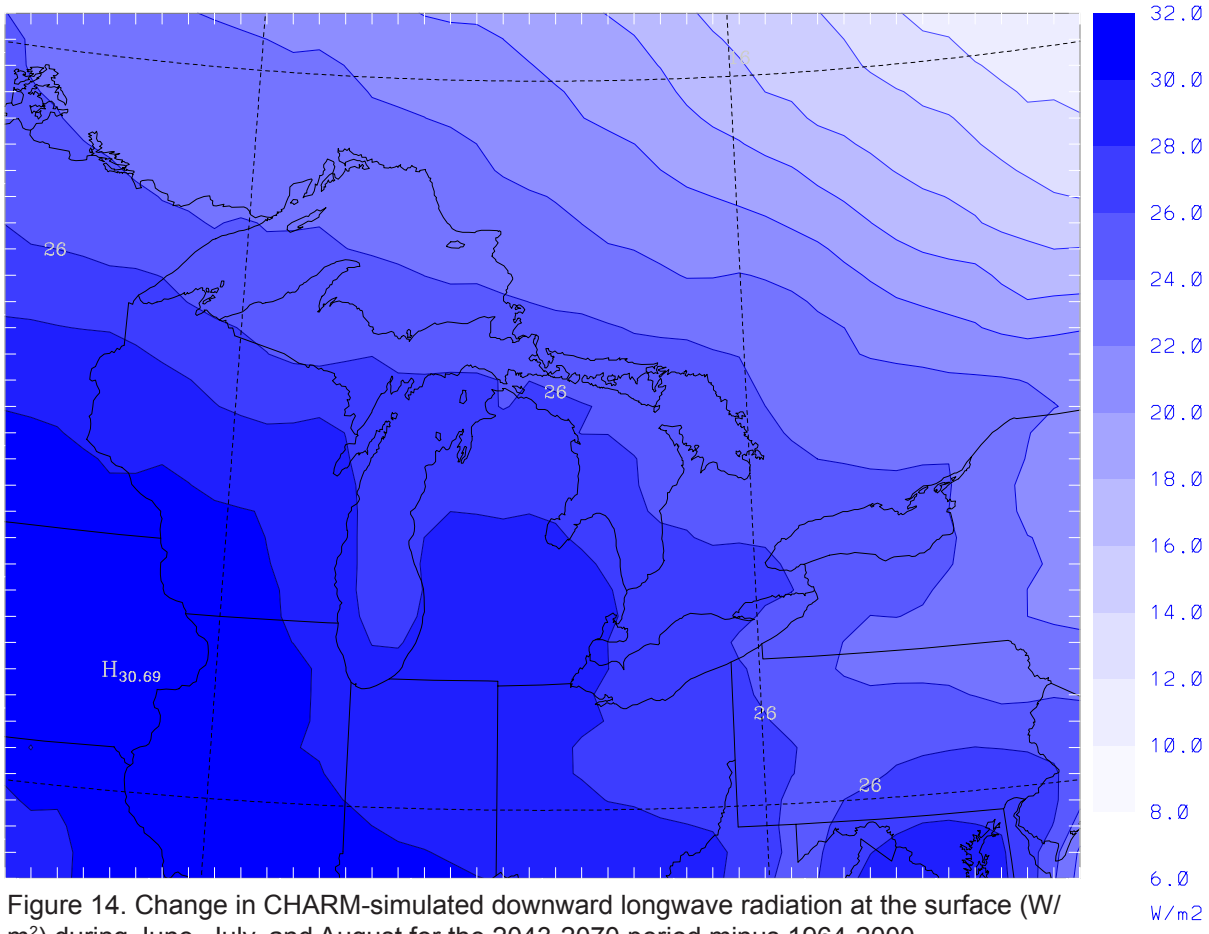

Figure 14. Change in CHARM-simulated downward longwave radiation at the surface (W/m^2) during June, July, and August for the 2043-2070 period minus 1964-2000.

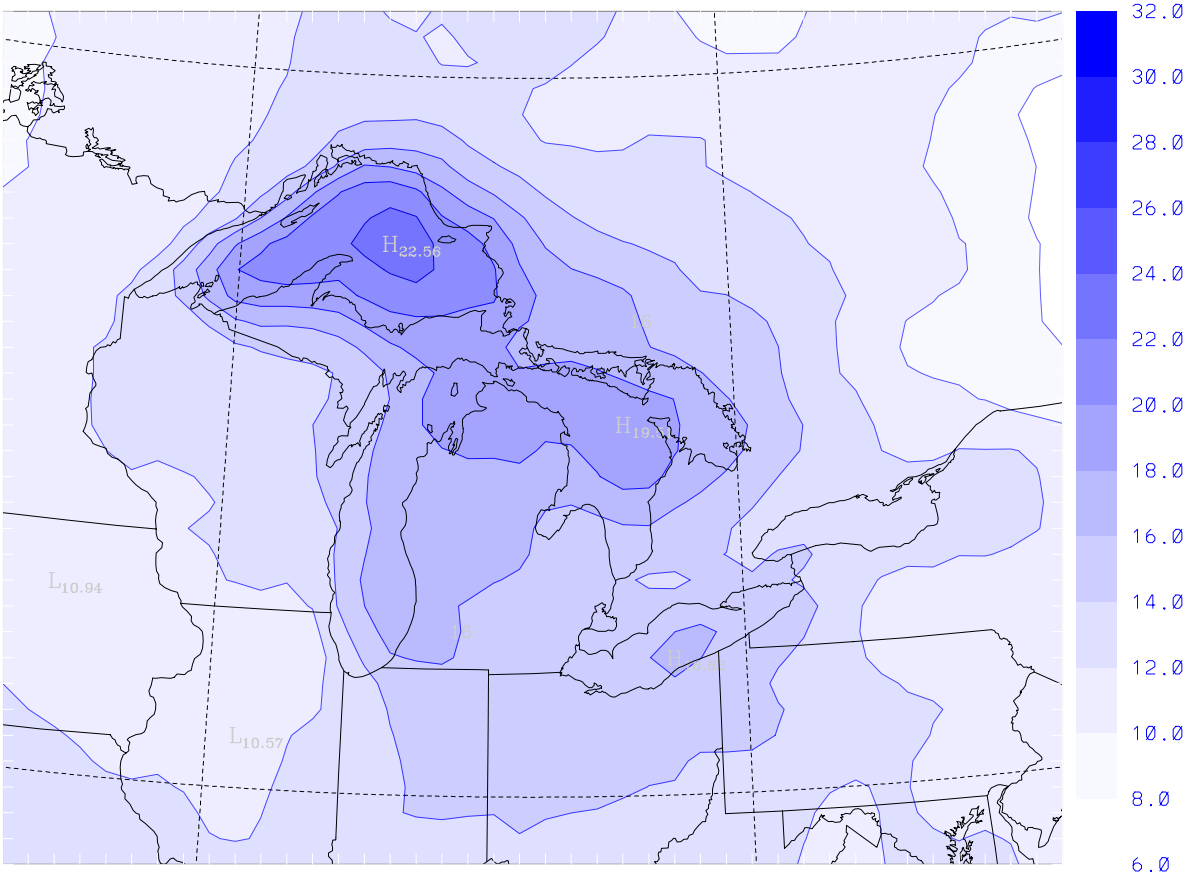

Figure 15. Change in CHARM-simulated downward longwave radiation at the surface (W/m^2) during December, January, and February for the 2043-2070 period minus 1964-2000.

5. LAKES TEMPERATURE AND ICE RESULTS

5.1 Lake surface temperature validation

As stated in section 2, the best results for the annual cycle of lake surface temperatures was found by using lake diffusion calculations based on multiplying simulated wind speeds at 47.7 m above ground level by a factor of 0.28 as a substitute for measured wind speeds at 2 m above ground (eq. 1). The resulting lake surface temperatures for representative lakes are shown in Fig. 16. On Lake Superior, the mean surface temperatures are very close to observations during late winter and early spring. During summer, they are biased warm, by as much as 6°C during June. During the fall and early winter, the bias switches to cold, but with magnitudes of about 2°C or less. In Lake Michigan, biases are mostly small, but are consistently cold in the range of August to January, with a maximum magnitude of about 4°C during November (notice the different scales between the two panels of Fig. 16).

5.2 Lake temperature profiles

Lake temperature profiles for central Lake Michigan (between 43° and 45° N latitude) differ markedly between the 1964-2000 period and the 2043-2070 period (Fig. 17). In addition to the general characteristic of warmer temperatures in the 2043-2070 period (red curves) than in 1964-2000 (blue curves), some months display special characteristics. Because of different bathymetry of the points that were averaged to obtain these plots, the group of points used to get temperatures in deep water is only a subset of those averaged to get shallow water temperatures. Therefore, the red curve in the panel representing February should be interpreted as showing a set of points with deep bathymetry having deep water temperatures greater than 4°C and stably stratified columns with warmer temperatures near the surface or neutrally stable columns with surface temperature equal to temperatures at depth. However, when the points with shallower water are included in the averaging, average water temperature near the surface is colder than at depth. This phenomenon also occurs in both profiles in the December panel.

A notable feature in Fig. 17 is that the temperatures in deep water during 2043-2070 are always greater than 4°C, and only in February are the surface temperatures marginally below this level. This means that, for most of the lake, mixing in the future case based on thermal instability does not occur when the water column passes through the 4°C threshold of maximum density in fall and spring, but rather occurs when the surface reaches its lowest temperature of the year. Furthermore, if that temperature is not as cold as previous years, the mixing may not reach the bottom. However, full-column mixing can still occur at locations with shallower bathymetry.

The panel for April shows that the future simulation has water positively stratified (i.e. warmest water near the surface), while the historical simulation has negative, or winter, stratification (coldest water on top). This means that the intense springtime mixing of the water column has already occurred in the future case, but not the historic case. Since this mixing carries nutrients from the deep water and sediments, its timing has important implications for the timing of plankton blooms in the spring, and affects the synchronization of this phenology with other components of the ecosystem.

Unfortunately, the results shown in Fig. 17 correspond poorly with the observations shown in McCormick et al. (2010). The numerics of the vertical mixing scheme seem to result in discrete mixing events, apparently encompassing only a single timestep, of which we have not yet been able to specifically detect one and dissect the calculations that lead to it. These result in the relatively homogeneous profiles in the October panel at temperatures well above 4°C (much warmer than in McCormick et al. 2010), as well as deep-water temperatures considerably above 4°C in August and even June. Plans for investigating and correcting this are discussed in section 6.

5.3 Lake ice cover

Increased greenhouse gases result in reduced ice cover. Lake Michigan's February ice cover is shown as an illustrative case (Fig. 18). Values above a 0.1 m threshold for mean ice thickness are necessary for ice to be depicted by a contour in Fig. 18; such areas are not extensive in the 1964-2000 period. But in the 2043-2070 time period, its extent is limited to a very small, shallow area at the northern end of Green Bay, as well as a small, shallow area in the northeastern part of the lake, near the Straits of Mackinac.

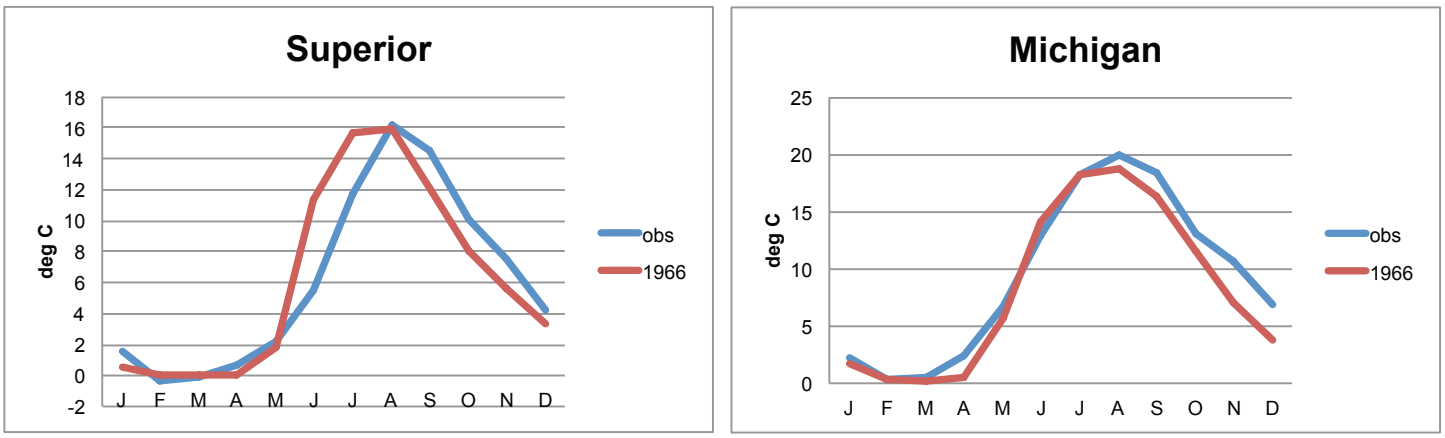

Figure 16. Area-mean annual cycle of lake surface temperatures from GLSEA observational data (blue) and CHARM simulations for the sub-period 1964-1968 (red, denoted as "1966") for Lake Superior (top) and Lake Michigan (bottom).

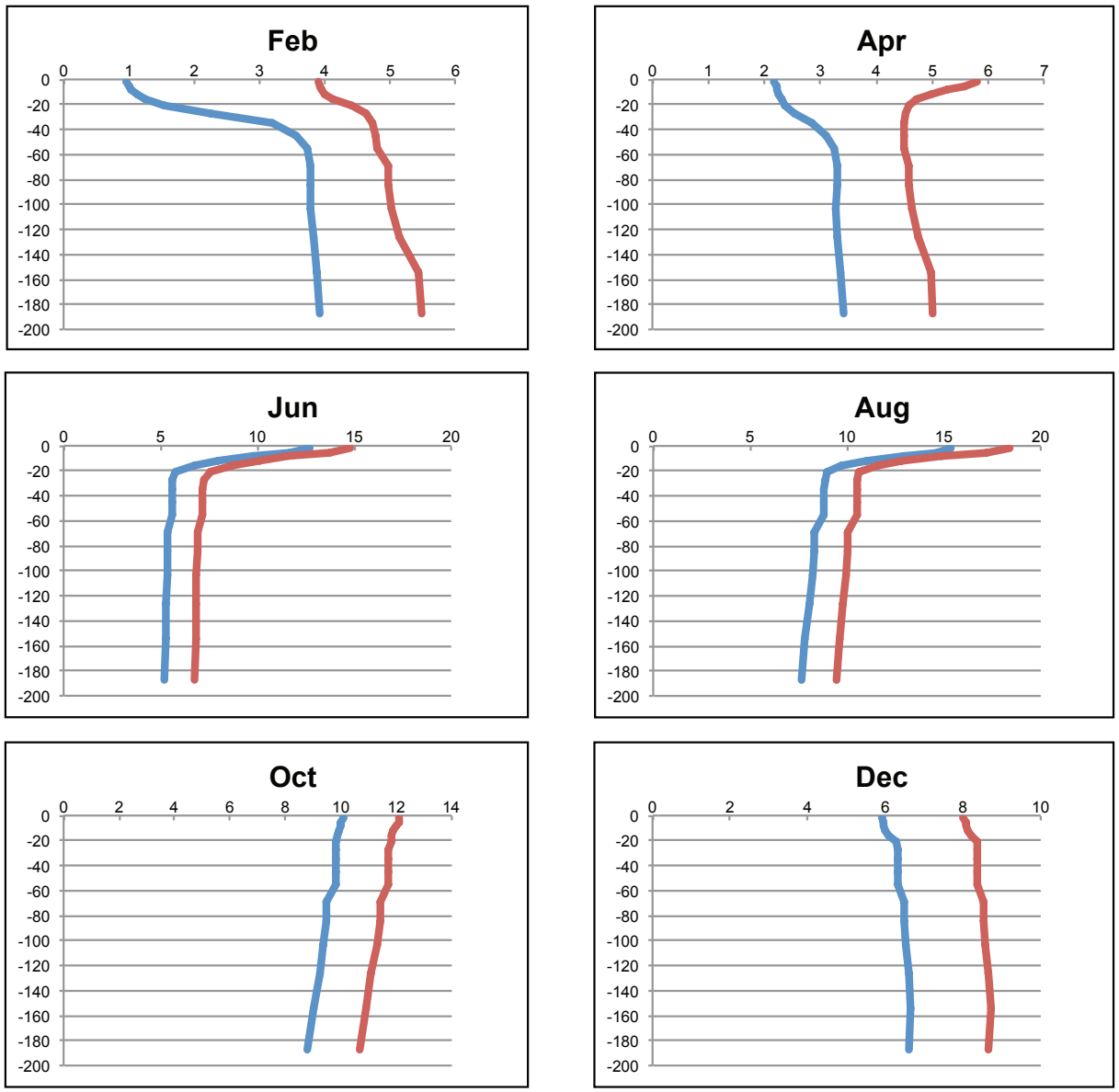

Figure 17. CHARM-simulated lake temperature profiles for central Lake Michigan (between 43° and 45° N) for various months. The blue curves are for the 1964-2000 period, and red curves for 2043-2070. The x-axis is temperature in degrees Celsius, and the y-axis is depth in meters.

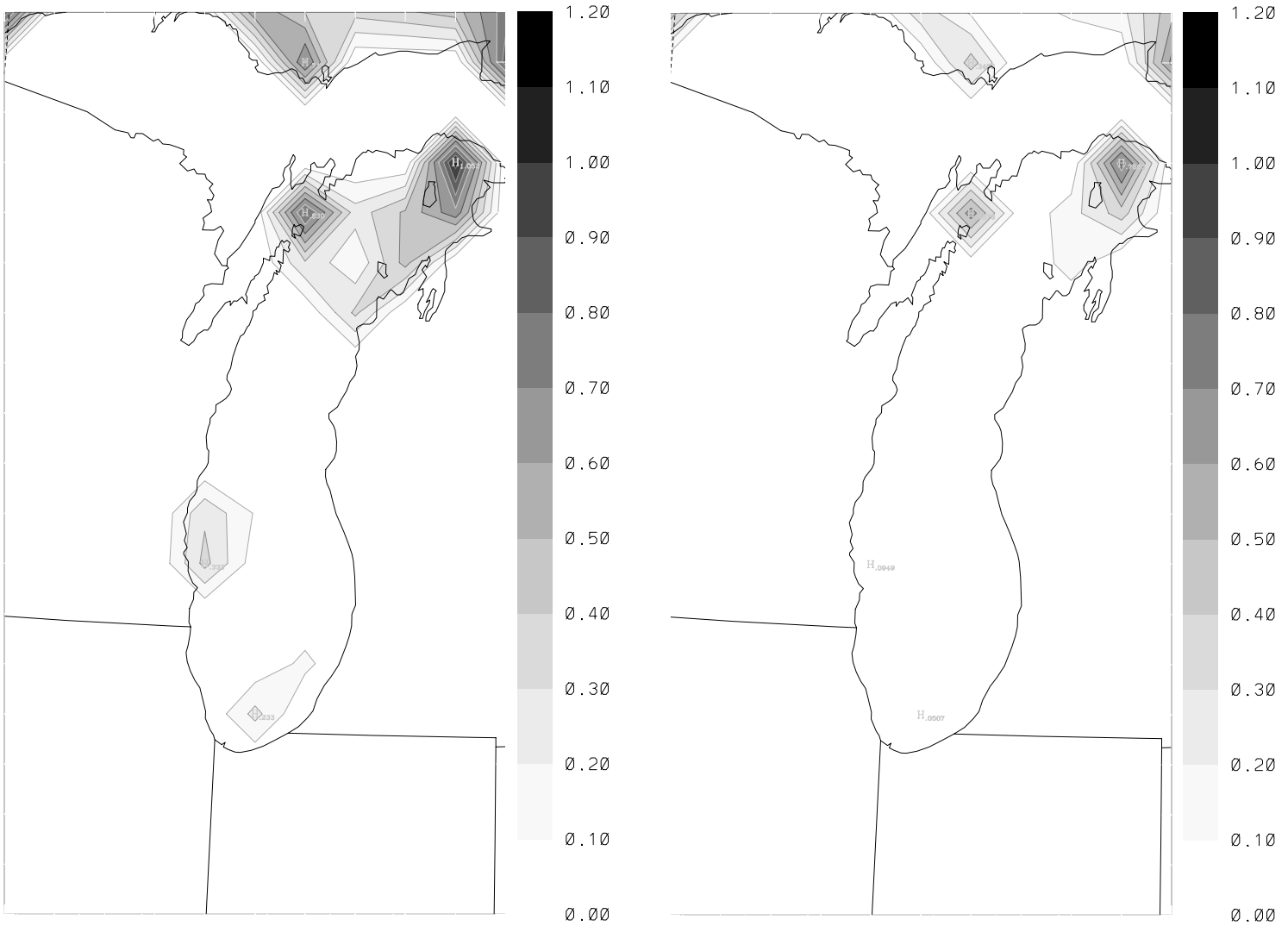

Figure 18. CHARM-simulated mean ice cover during February for Lake Michigan in the 1964-2000 case (left) and 2043-2070 (right).

6. DISCUSSION, CONCLUSIONS, AND FUTURE PLANS

A variety of results of GHG-induced climate change are simulated in the Great Lakes region using the CHARM model. One of the most basic is near-surface air temperature. This increases in both summer and winter, and the summer has a particular phenomenon of smaller magnitude of air temperature increase directly over the lakes. We hypothesize that this reduced temperature increase is due to changes in fog over the lakes, and consequences involving transfer of longwave radiation among the surface, boundary layer, and free atmosphere. However, the very frequent existence of fog over the lakes during the summer is an unrealistic prediction of CHARM.

Precipitation is projected to generally increase in the future, with the strongest systematic increases occurring during winter in the lake effect zones. That is, the near-lake areas that already receive much winter precipitation will be the focus of increases. Unfortunately, precipitation in the historical time period does not validate well against observations. Evapotranspiration increases in the future, most intensely over the lakes during the winter. The magnitude of increased ET over land is weak. We did not analyze the net effect of precipitation and ET, both because of the strong bias in precipitation and because of suspected problems with the system to account for runoff and percolation. Therefore, projected lake levels are not included in this report. In the future, we would like to supplement direct analysis of runoff and percolation with analysis of atmospheric moisture flux convergence, similar to what was done in Kutzbach et al. (2005).

Changes in near-surface wind do not seem to be very systematic. During summer, there is some increase in the anti-cyclonic (clockwise) circulation associated with the lakes. And during the winter, especially in the eastern Great Lakes, the magnitude of prevailing westerly winds is reduced.

Downward longwave radiation, the starting point of the greenhouse effect, is increased in the future. The magnitude of this is larger overall during the summer, but in the winter, it is especially strong over the lakes. Future analysis in terms of the height of the boundary layer and capping stratus clouds may shed more light on this.

Water temperatures increase during the future. Notably, the timing of the onset of positive stratification (warmer water overlying colder water) is earlier, implying that the overturning that is an effective means of bringing nutrients closer to the surface occurs earlier, with potential ecological ramifications. Ice is considerably reduced, and is likely to be confined to shallow parts of the lakes.

As in Lofgren et al. (2011), we emphasize that responses in aspects of the lake and land surface in the presence of enhanced CO_2 concentrations should not be interpreted as simply resulting from air temperature. Instead, human-released greenhouse gases act as the first step in generating changes throughout a web of interactions. For example, downward longwave radiation is the aspect that is most directly influenced by CO_2 concentration, and will directly influence surface temperature (both land and lakes). But at the same time, it is influenced by feedbacks from air temperature, humidity, and clouds. Likewise, temperatures of land surfaces and lakes, evapotranspiration, lake ice cover, precipitation, and many other phenomena should not be regarded as resulting from climate change, but as aspects of climate change themselves. Particular bugs and shortcomings in CHARM have been identified. For purposes of completing the current project and creating a model run, these have been left intact and the contents in this report reflect CHARM as it existed with these problems. The following will be addressed in the future:

- The error in coding of the eddy diffusivity, where the formula for Brunt-Vaisala frequency is erroneously squared a second time (fourth power) will be corrected. This will create a new environment for tuning of the coefficient by which the wind speed at the lowest model level is multiplied within the formula for Richardson-number dependent diffusivity; therefore, this tuning will be repeated for future model runs.

- The diffusion of temperature within the water column seems to consist of the expected diffusion of temperature that is gradual and continuous in time, in addition to discrete episodic mixing events that are likely not associated with very strong wind events. Temporary fixes have ensured that heat energy is conserved during these events, and that they do not result in a statically unstable water column, but either neutrally or positively stable at all depths. However, in order to diagnose these episodes and find their causes within the model's numerics, it is necessary to find a time and place at which one of these episodes occurs, carefully pull apart the calculations that lead to it, and fix the problem as appropriate.

- Fog over the Great Lakes during summer is occurring in the model on an unrealistically frequent basis. We need to figure out a reasonable way to increase the atmospheric boundary layer's vertical diffusion, especially when lake surface conditions lead to strong static stability between the lowest and next-lowest layers of the model, in order to reduce this recurring, persistent, and self-reinforcing fog.

- When using the CRCM data, in turn based on the CGCM3 data, as lateral boundary conditions, the precipitation amounts are severely dry-biased. It is hoped that other GCM and reanalysis input datasets will produce more satisfactory results. In addition, more tuning of the convective precipitation may help this situation, especially because the biases are most severe during the convective precipitation-dominated summertime. Making the convective precipitation scheme more active may also reduce the occurrence of over-lake fog by decreasing the moist static energy of the low-level air advecting over the lakes, and consequently reducing the static stability between the very lowest model layer and layers above it, as well as reducing the water vapor mixing ratio of the air advecting over the lakes.

- The post-processing tools to calculate net basin supply need to be carefully validated, both for self-consistency (i.e. carry the units through the set of calculations accurately) and comparison to observed streamflow and net basin supply calculated by a residual method.

In parallel with these ongoing development steps for CHARM, Dr. Lofgren is also cooperating with Dr. Chuliang Xiao of the Cooperative Institute for Limnology and Ecosystems Research to develop a conceptually similar model for the Great Lakes basin, based on the Weather Research and Forecasting (WRF) Model. WRF is much more widely used at present and far more actively supported by a large group of developers and users.

Acknowledgments. Thanks to Michael Notaro, Carlo DeMarchi, Chuliang "Andy" Xiao, and John Bratton for discussions that were useful in creating this report. This work was partially supported by the International Joint Commission's Upper Great Lakes Study, the Environmental Protection Agency's Great Lakes Restoration Initiative, and the US Geological Survey's National Climate Change and Wildlife Science Center. Computing facilities were provided by the NOAA Earth System Research Laboratory.

7. REFERENCES

Angel, J.R., and K.E. Kunkel, 2010: The response of Great Lakes water levels to future climate scenarios with an emphasis on Lake Michigan-Huron. *J. Great Lakes Res*., 36, Supplement 2, 51-58.

Austin, J.A., and S.M. Colman, 2007: Lake Superior summer water temperatures are increasing more rapidly than regional air temperatures: A positive ice-albedo feedback. *Geophys. Res. Lett*., 34, doi: 10.1029/2006GL029021.

Avissar, R., and R.A. Pielke, 1989: A parameterization for heterogeneous land surfaces for atmospheric numerical models and its impact on regional meteorology. *Mon. Wea. Rev*., 117, 2113-2136.

Bennington, B., M. Notaro, and K.D. Holman, 2014: Improving climate sensitivity of deep lakes within a regional climate model and its impact on simulated climate. *J. Climate*, 27, 2886-2911, doi:10.1175/JCLI-D-13-00110.1.

Cotton, W.R., and Coauthors, 2003: RAMS 2001: Current status and future directions. *Meteor. Atmos. Phys*., 82, 5-29.

Croley, T.E., II, 1983: Great Lake basins (U.S.A.-Canada) runoff modeling. *J. Hydrology*, 64, 135-158.

Croley, T.E., II, 1990: Great Lakes double-CO_2 climate change hydrological impacts. *Climatic Change*, 17, 27-47.

de Elia, R., and H. Côté, 2010: Climate and climate change sensitivity to model configuration in the Canadian RCM over North America. *Meteorologische Zeitschrift*, 19, 1-15.

Flato, G. M., and G. J. Boer, 2001: Warming asymmetry in climate change simulations. Geophys. Res. Lett., 28, 195-198.

Gula, J., and W.R. Peltier, 2012: Dynamical downscaling over the Great Lakes basin of North American using the WRF regional climate model: The impact of the Great Lakes system on regional greenhouse warming. *J. Climate*, 25, 7723-7742, doi:10.1175/JCLI-D-11-00388.1.

Hartmann, H.C., 1990: Climate change impacts on Laurentian Great Lakes levels. *Climatic Change*, 17, 49-67.

Hayhoe, K., J. VanDorn, T. Croley II, N. Schlegal, and D. Wuebbles, 2010: Regional climate change projections for Chicago and the Great Lakes. *J. Great Lakes Res.*, 36, Supplement 2, 7-21.

Hostetler, S.W., and P.J. Bartlein, 1990: Simulation of lake evaporation with application to modeling lake level variations of Harney-Malheur Lake, Oregon. *Wat. Resour. Res*., 26, 2603-2612.

IPCC, 2000: Special Report on Emission Scenarios, Nakicenovic, N., and R. Swart, eds. Cambridge University Press, Cambridge, UK.

IPCC, 2013: Climate Change 2013: The Physical Science Basis. Contribution of Working Group I to the Fifth Assessment Report of the Intergovernmental Panel on Climate Change, Stocker, T. F., D. Qin, G.-K. Plattner, M. Tignor, S. K. Allen, J. Boschung, A. Nauels, Y. Xia, V. Bex, and P. M. Midgley, eds. Cambridge University Press, Cambridge, UK, and New York, USA, 1535 pp.

Kutzbach, J.E., J.W. Williams, and S J. Vavrus, 2005: Simulated 21st-century changes in regional water balance of the Great Lakes region and links to changes in global temperature and poleward moisture transport. *Geophys. Res. Lett*., 32, L17707, doi:10.1029/2005GL023506.

Lofgren, B.M., 2004: A model for simulation of the climate and hydrology of the Great Lakes basin. *J. Geophys. Res.*, 109, D18108, doi:10.1029/2004JD004602.

Lofgren, B.M., T.S. Hunter, and J. Wilbarger, 2011: Effects of using air temperature as a proxy for evapotranspiration in climate change scenarios of Great Lakes basin hydrology. *J. Great Lakes Res*., 37, 744-752, doi:10.1016/j.jglr.2011.09.006.

MacKay, M., and F. Seglenieks, 2013: On the simulation of Laurentian Great Lakes water levels under projections of global climate change. *Climatic Change*, 117, 55-67.

Manabe, S., R.T. Wetherald, P.C.D. Milly, T.L. Delworth, and R.J. Stouffer, 2004: Century-scale change in water availability: CO_2-tripling experiment. *Climatic Change*, 64, 59-76.

McCormick, M. J., Z. Li, D. J. Schwab, and S. A. Ruberg, 2010: Lake Michigan vertical temperature data—midlake 1991-2009. NOAA GLERL Technical Memorandum TM-150. Data available at: http://www.glerl.noaa.gov/ftp/publications/tech_reports/glerl-150/appendix1/

Mearns, L.O., W.J. Gutowski, R. Jones, L.-Y. Leung, S. McGinnis, A.M.B. Nunes, and Y. Qian, 2009: A regional climate change assessment program for North America. *Eos*, 90, 311-312.

Milly, P.C.D., K.A. Dunne, and A.V. Vecchia, 2005: Global pattern of trends in streamflow and water availability in a changing climate. *Nature*, 438, 347-350.

Music, B., and D. Caya, 2007: Evaluation of the hydrological cycle over the Mississippi River basin as simulated by the Canadian Regional Climate Model (CRCM). *J. Hydrometeorology*, 8, 969-988.

Music, B., A. Frigon, B. Lofgren, R. Turcotte, and J.-F. Cyr, 2014: Present and future Laurentian Great Lakes hydroclimatic conditions and associated water supplies as simulated by regional climate models. *J. Great Lakes Res*., submitted.

Niziol, T.A., W.R. Snyder, and J.S. Waldstreicher, 1995: Winter weather forecasting throughout the eastern United States. Part IV: Lake effect snow. *Wea. Forecasting*, 10, 61-77.

Notaro, M., V. Bennington, and S. Vavrus, 2014: Dynamically downscaled projections of lake-effect snow in the Great Lakes basin. *J. Climate* (submitted.)

Pielke, R. A., and Coauthors, 1992: A comprehensive meteorological modeling system--RAMS. *Meteor. Atmos. Phys*., 49, 69-91.

Sousounis, P.J., and J.M. Fritsch, 1994: Lake-aggregate mesoscale disturbances. Part II: A case study of the effects on regional and synoptic-scale weather systems. *Bull. Amer. Meteorol. Soc*., 75, 1793-1811.

Tremback, C.J., 2005: RAMS: The Regional Atmospheric Modeling System--Technical Description. http://www.atmet.com/html/docs/rams/rams_techman.pdf

Tremback, C.J., and R. Kessler, 1985: A surface temperature and moisture parameterization for use in mesoscale numerical models. Preprints, 7th Conference on Numerical Weather Prediction, 17-20 June 1985, Montreal, Quebec, Canada, American Meteorological Society.